



Contents lists available at ScienceDirect

Spectrochimica Acta Part A: Molecular and Biomolecular Spectroscopy

journal homepage: www.elsevier.com/locate/saa

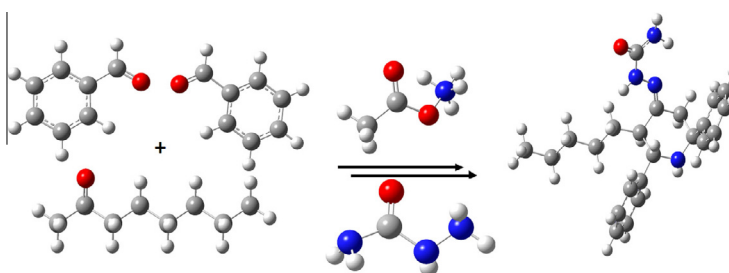
Synthesis, spectroscopic (FT-IR, FT-Raman, UV and NMR) and computational studies on 3*t*-pentyl-2*r*,6*c*-diphenylpiperidin-4-one semicarbazone

M. Arockia doss^a, S. Savithiri^a, G. Rajarajan^{a,*}, V. Thanikachalam^a, H. Saleem^b^a Department of Chemistry, Annamalai University, Annamalainagar 608 002, India^b Department of Physics, Annamalai University, Annamalainagar 608 002, India

HIGHLIGHTS

- Conformational analysis.
- *Ab initio* HF and DFT calculations.
- Tentative assignments are made based on the TED values.
- The theoretical UV–visible spectrum has a good concordance with the experimental one.
- The calculated ¹H and ¹³C chemical shifts are in good agreement with the experimental ones.

GRAPHICAL ABSTRACT



ARTICLE INFO

Article history:

Received 15 August 2014

Received in revised form 11 March 2015

Accepted 27 March 2015

Available online 3 April 2015

Keywords:

Semicarbazone

HOMO–LUMO

NBO

NLO

NMR

ABSTRACT

The structural and spectroscopic studies of 3*t*-pentyl-2*r*,6*c*-diphenylpiperidin-4-one semicarbazone (PDPOSC) were made by adopting B3LYP/HF levels theory using 6-311++G(d,p) basis set. The FT-IR and Raman spectra were recorded in solid phase, the fundamental vibrations were assigned on the basis of the total energy distribution (TED) of the vibrational modes, calculated with scaled quantum mechanics (SQM) method and PQS program. DFT method indicates that B3LYP is superior to HF method for molecular vibrational analysis. UV–vis spectrum of the compound was recorded in different solvents in the region of 200–800 nm and the electronic properties such as excitation energies, oscillator strength, wavelengths, HOMO and LUMO energies were evaluated by time-dependent DFT (TD-DFT) approach. The polarizability and first order hyperpolarizability of the title molecule were calculated and interpreted. The hyperconjugative interaction energy ($E^{(2)}$) and electron densities of donor (i) and acceptor (j) bonds were calculated using NBO analysis. In addition, MEP and atomic charges of carbon, nitrogen and oxygen were calculated using B3LYP/6-311++G(d,p) level theory. Moreover, thermodynamic properties of the title compound were calculated by B3LYP/HF, levels using 6-311++G(d,p) basis set. The ¹H and ¹³C nuclear magnetic resonance (NMR) chemical shifts of the molecule were calculated by the gauge independent atomic orbital (GIAO) method and compared with experimental results.

© 2015 Elsevier B.V. All rights reserved.

Introduction

Piperidine ring is one of the important structural entities among heterocyclic molecules [1]. Attention has been focused on structure–activity relationship of such compounds. Primarily systems

having piperidin-4-one nucleus have aroused great interest in the past and also in recent years due to their biological activities like antiviral [2], antitumor [3], antiinflammatory [4], central nervous system [5], anticancer [6] and antibacterial activity [7]. Piperidines with substituents at C3 and C5 have increased biological activity compared to other piperidines. Non-linear optical (NLO) materials play a vital role in the field of fiber optic communications and optical signal process. In the last two decades,

* Corresponding author. Tel.: +91 9444147388.

E-mail address: rajarajang70@gmail.com (G. Rajarajan).

intensive research has shown that organic crystals also exhibit nonlinear optical efficiencies which are of greater magnitude than those of inorganic materials. Semicarbazones and thiosemicarbazone of substituted heterocyclic organic compounds, ketones and acetophenones were reported to be potential organic NLO [8–10] materials.

Now a days NIR-FT-Raman spectrographic analysis combined with quantum chemical computations are employed as an effective tool in the vibrational analysis of biological compounds [11,12] and natural products, since fluorescence-free Raman spectra and the computed results can help unambiguous identification of vibrational modes and also as the bonding and structural features of complex organic molecular systems. The present study aimed at to investigate the molecular structural properties, vibrational and energetic data of PDPOSC, in gas phase, due to its pharmaceutical importance. The ground and the excited state properties of the title molecule are calculated using DFT/B3LYP and HF levels of theories using 6-311++G(d,p) basis set. As vibrational and electronic spectroscopic studies provide very useful information about the structure and conformation of the molecules if used in synergy with quantum chemical calculations, to obtain a complete description of molecular dynamics, vibrational wavenumber calculation along with the normal mode analysis has been administered at the DFT/HF level theories. The investigation of geometry, dipole moment, polarizability, first static hyperpolarizability, along with the molecular electrostatic potential surface will lead to better understanding of the structural and spectral characteristics of the compound chosen for study.

Experimental details

Synthesis of 3*t*-pentyl-2*r*,6*c*-diphenylpiperidin-4-one semicarbazone

3*t*-pentyl-2*r*,6*c*-diphenylpiperidin-4-one was synthesized as per the procedure described in literature [13]. Semicarbazone derivative of 3*t*-pentyl-2*r*,6*c*-diphenylpiperidin-4-one was prepared by the reaction of the ketone with semicarbazide hydrochloride. To a solution of 3*t*-pentyl-2*r*,6*c*-diphenylpiperidin-4-one (0.01 mol) in 45 mL methanol and few drops of conc. HCl were added. Then, semicarbazide (previously dissolved in 20 mL methanol) solution (0.01 mol) was added drop wise with stirring. The reaction mixture was refluxed for 3 h on a heating mantle. After cooling, the solid product was filtered off and recrystallized from 20 mL methanol. Yield 75%; m.p.: 154 (°C); MF: C₂₃H₃₀N₄O; Elemental analysis: Calcd (%): C, 72.98; H, 7.99; N, 14.80; found (%): C, 72.93; H, 7.70; N, 14.89.

Spectral measurements

The FT-IR spectrum of the synthesised piperidone semicarbazone was measured in the range 4000–500 cm⁻¹ in AVATAR-330 FT-IR spectrometer (Thermo Nicolet) using KBr (pellet form) in the Department of Chemistry, Annamalai University, Annamalainagar. The FT-Raman spectrum of PDPOSC has been recorded using 1064 nm line Nd:YAG laser with excitation wavelength of 1064 nm in the region 100–4000 cm⁻¹ on a thermo Electron corporation model Nexus 670 spectrophotometer equipped with FT-Raman module accessory. The FT-Raman spectrum was taken at Central Electro Chemical Research Institute, Karaikudi, Tamilnadu. Microanalyses were performed on VarioMicro V2.2.0 CHN analyser. ¹H NMR spectrum was recorded at 400 MHz and ¹³C NMR spectrum at 100 MHz on a BRUKER model using CDCl₃ as solvent. Tetramethylsilane (TMS) was used as internal reference for all NMR spectra, with chemical shifts reported in δ units (parts per million) relative to the standard.

Computational details

The combination of vibrational spectroscopy with quantum chemical calculations is effective for understanding the fundamental modes of vibrations of compounds. The structural characteristics, stability, thermodynamic properties of the compound under investigation are determined by B3LYP and HF levels theories, using 6-311++G (d,p) basis set in Gaussian 03W program [14]. The optimized structural parameters were used in the vibrational frequency calculations resulting in IR and Raman frequencies along with intensities and Raman depolarization ratios, thermodynamic properties and energies of the optimized structures. The vibrational modes were allotted on the premise of TED analysis using SQM program [15]. HF and DFT hybrid B3LYP functional methods tend to overestimate the fundamental modes and hence the scaling factors 0.9608 and 0.9051 [16] have been uniformly applied to the B3LYP and HF methods, respectively.

To investigate the reactive sites of the title molecule, the molecular electrostatic potential was evaluated. Moreover, in order to show nonlinear optical (NLO) activity of PDPOSC molecule, the dipole moment, linear polarizability and first order hyperpolarizability were obtained from molecular polarizabilities based on theoretical calculations. The electronic properties, such as HOMO–LUMO energies were calculated using TD-DFT/6-311++G(d,p) based on the optimized structure in gas phase and in solvents (methanol and chloroform). NBO [14] analysis was carried out so as to elucidate inter- and intramolecular interactions in the title molecule. Raman intensities were calculated by the procedure described in literature [17].

Results and discussion

Conformational analysis

In piperidone derivatives the most stable conformer is the chair form [18–20]. The semicarbazone analogue has rotatable bonds, and so several conformers (Fig. S1) are possible for PDPOSC. These structures were subjected to more accurate computations using B3LYP/6-311++G(d,p) and the ground state energy, energy difference and dipole moment of conformers are presented in Table 1.

From the calculated energies the conformer 1 is found to be more stable. In order to explain conformational flexibility of the stable conformer, the energy profile as a function of H–C–C torsional angle is shown in Fig. 1. All the geometrical parameters were at the same time relaxed throughout the calculations whereas the H–C–C torsional angle was varied in steps of 10°. The torsional potential surface of molecule was obtained by using semi-empirical (Austin Model, AM1) methodology. As can be seen from Fig. 1, the foremost conformer is with 180° (and –180°) torsional angle (H37–C35–C3–C4). A local minima was obtained for 10°. The optimized geometry of the molecule is coplanar.

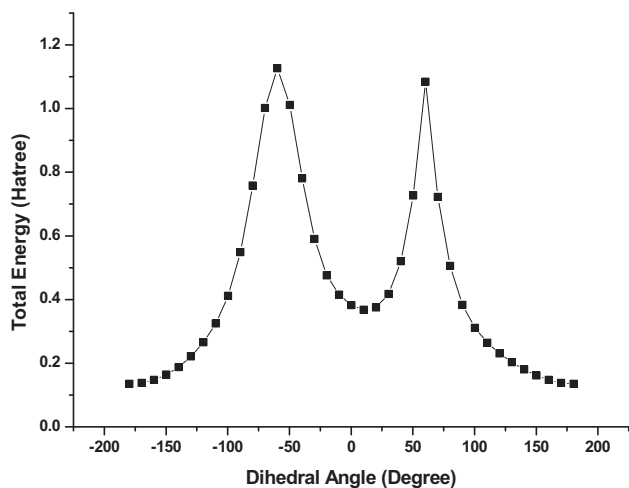
Molecular geometry

The optimized structural parameters such as bond lengths, bond and dihedral angles of PDPOSC were determined at B3LYP/HF level theories with 6-311++G(d,p) basis set and are presented in Table S1 in accordance with the atom numbering scheme of the molecule shown in Fig. 2. To the best of our knowledge, no single crystal X-ray crystallographic data of PDPOSC has yet been reported. However, the theoretical results obtained are almost comparable with closely related molecules such as 3*t*-pentyl-2*r*,6*c*-diphenylpiperidine-4-one [21] and (*E*)-2-(hexan-2-ylidene)hydrazinecarboxamide [22].

Table 1

Calculated energies and energy differences of possible conformers of the PDPOSC by DFT (B3LYP/6-311++G(d, p)) method.

Conformers	Energy		Energy differences		Dipole moment (Debye)
	(Hartree)	(kcal/mol)	(Hartree)	(kcal/mol)	
Conf-1	-1189.05932	-746146.61	0	0	4.52
Conf-2	-1189.04865	-746139.92	-0.0106688	-6.6948	4.50
Conf-3	-1189.04831	-746139.7	-0.0110072	-6.9071	3.97
Conf-4	-1189.04665	-746138.66	-0.0126688	-7.9498	4.49
Conf-5	-1189.04249	-746136.05	-0.0168298	-10.561	4.79
Conf-6	-1189.04065	-746134.9	-0.0186688	-11.715	4.27
Conf-7	-1189.03097	-746128.82	-0.0283503	-17.79	5.77
Conf-8	-1188.78092	-745971.92	-0.2783955	-174.7	4.01

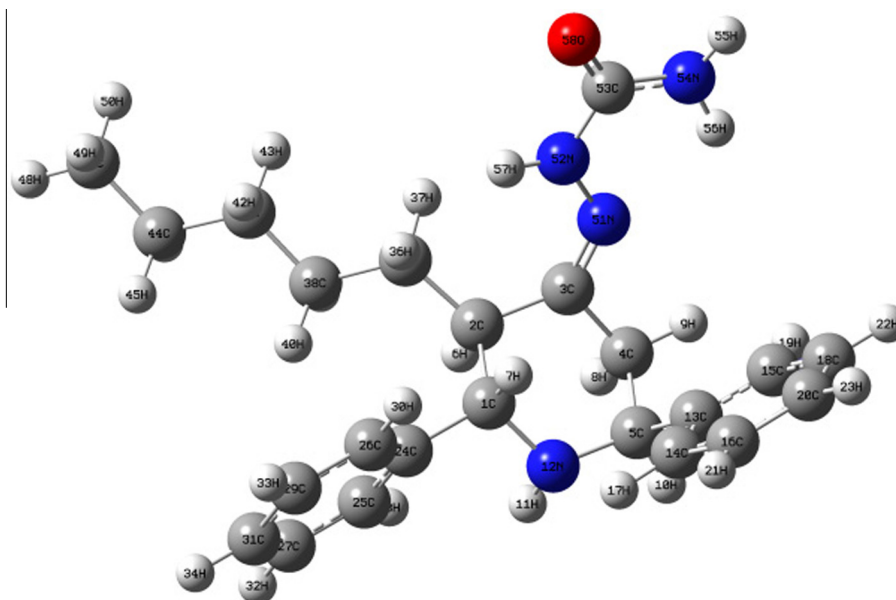
**Fig. 1.** Potential energy surface scan of PDPOSC with dihedral angle H37–C35–C3–C4.

The calculated C–C bond distance in the piperidine ring is in the range 1.511–1.567 Å by HF/6-311++G(d,p) nearly coincides with experimental value 1.550–1.56 Å [21]. The C–C mean bond lengths of the benzene rings are 1.3949 (B3LYP) and 1.3862 Å (HF). The computed value by HF/6-311++G(d,p) shows excellent agreement with XRD value 1.388 Å. Literature value for C–H bond distance

is ~ 1 Å. The predicted bond length lies between 1.0887–1.0986 Å (B3LYP) and 1.0797–1.0892 Å (HF) for heterocyclic ring. The average bond distance of C1–N12 and C5–N12 are 1.471 and 1.461 Å by B3LYP and HF, respectively in which B3LYP value is in line with literature value 1.471 Å [21]. The N52–C53–O58 and N54–C53–O58 angles are found to be 120.04 and 125.33° (B3LYP) and 120.07 and 124.19° (HF). Difference within the values are as a result of inter- and intramolecular hydrogen bonding. The lengthening of N54–H56 bond by about 0.138 Å/B3LYP and 0.121 Å/HF and shortening of C53–O58 bond by about 0.031 Å (B3LYP) and 0.033 Å (HF) indicate the possibility of N54–H56...O58 hydrogen bonding. Piperidine ring essentially adopts chair conformation, with all substituents equatorial as evident from the torsional angles N12–C1–C2–C3 = -54.21, -55.70 and -51.99 and N12–C5–C4–C3 = 51.26°, 52.43° and 54.81° by B3LYP, HF and XRD, respectively. In the molecular optimized structure, the semicarbazone analogue is nearly planar with the dihedral angle (N51–N52–C53–N54) 11.23° (B3LYP) and 17.77° (HF) and adopts an *E* configuration with respect to the C3=N51 bond.

Vibrational analysis

The FT-IR and FT-Raman spectra of PDPOSC are shown in Figs. S2 and S3. The observed and calculated frequencies by B3LYP and HF levels using 6-311++G(d,p) basis set along with their relative intensities, probable assignments and total energy distribution (TED) of the compound are summarized in Table 2.

**Fig. 2.** Optimized geometry of PDPOSC with atoms numbering calculated by B3LYP/6-311++G(d,p).

N–H vibrations

It is stated that in amines, the N–H [23] stretching vibrations occur in the region 3500–3300 cm^{-1} . With the above reference, the vibrational frequency observed at 3461 cm^{-1} in the infrared spectrum is assigned to the $-\text{NH}_2$ stretching mode, the corresponding computed value matches at 3453 and 3509 cm^{-1} by B3LYP and HF, respectively (mode no.: 167). Moreover the N–H stretching vibration appears as pure mode at the mode numbers 166 and 165 as calculated 3448 and 3421 cm^{-1} and 3477 and 3433 cm^{-1} by B3LYP and HF, respectively. The TED corresponding to this vibration contributes to about 99%. The in-plane bending mode of H–N–H is 1353 cm^{-1} in FT-IR and 1522 cm^{-1} in FT-Raman, these vibrations are in line with the calculated values 1356, 1524 cm^{-1} (mode nos: 117,132) in B3LYP level theory.

C=O, C=N, C–N vibrations

The C=O [24] stretching lies in the spectral range 1750–1860 cm^{-1} and is very intense in the infrared and moderately active in Raman. In PDPOSC, the carbonyl stretching frequency is observed in the high frequency region as a very strong band at 1691 cm^{-1} in IR and medium band at 1685 cm^{-1} in Raman spectrum and the same band computed by 1695/B3LYP and 1713 cm^{-1} /HF (mode no.: 137) level theory. The TED analysis shows 72% of contribution. In 3-methyl-2,6-diphenylpiperidin-4-ylidene semicarbazide, the carbonyl stretching frequency is observed as a very strong band at 1695 cm^{-1} in IR [23]. The C–N extending wavenumber is noticeably troublesome as there are issues in distinguishing these wavenumbers from other different vibrations. Dhandapani et al. [23] assigned C–N stretching absorption in the region 1603 cm^{-1} in 3-methyl-2,6-diphenylpiperidin-4-ylidene semicarbazide. In the present work, the C–N band observed at 1649 cm^{-1} in FT-IR spectrum (1600 cm^{-1} in FT-Raman), whereas the theoretically computed value of C–N stretching vibration is 1650 cm^{-1} /B3LYP and 1655 cm^{-1} /HF (mode no.: 136), respectively. The B3LYP value is in concurrence with experimental observation and its TED value 78%. In the present investigation, the C–N bending vibration observed at 1444 and 1442 cm^{-1} /B3LYP and 1475 and 1467 cm^{-1} /HF (mode no.: 127 and 125), respectively. In benzamide, the band observed at 1368 cm^{-1} is assigned to C–N stretching [25], in Benzotriazole [26] the C–N stretching bands are found at 1307 and 1382 cm^{-1} . The theoretically computed wavenumber falls in the region 1350–1207 cm^{-1} for PDPOSC molecule. The TED corresponding to the vibrations is ~30% mixed with the stretching vibration as shown in Table 2.

Methyl and methylene group vibrations

PDPOSC under consideration possesses a CH_3 group in the side chain. C–H stretching in CH_3 occurs at lower frequencies than those of aromatic ring (3100–3000 cm^{-1}). The asymmetric C–H stretching mode of CH_3 is expected at 2870 cm^{-1} [27,28]. In the present study, the C–H asymmetric stretching vibration appears as medium to weak bands at 2955 cm^{-1} in FT-IR. The theoretically predicted value by B3LYP method 2960 cm^{-1} (mode no.: 151) shows good concurrence with the experimental observations. The C–H symmetric stretching vibration is seen in FT-IR at 2927, 2856 cm^{-1} and in FT-Raman at 2930 cm^{-1} . The C–H symmetric stretching mode predicted by B3LYP method shows the range from 2927–2870 cm^{-1} and by HF method shows the range from 2939–2840 cm^{-1} (mode nos.: 149–139). These vibrations are supported by TED values (10–84%).

Aromatic C–H vibrations

For simplicity, modes of vibrations of aromatic compounds is considered separately as C–H or ring C–C vibrations. However, as with any complex molecule, vibrational interactions happen and these levels just show the predominant vibration. Substituted benzenes have large number of sensitive bands, i.e., bands whose position is significantly influenced by the mass and electronic properties, mesomeric or inductive effect of the substituent. As indicated in literature [29,30], in infrared spectra, most aromatic compounds have peaks in the region 2900–3100 cm^{-1} , these are because of the stretching vibrations of the ring C–H bands. In the present study, the FT-IR bands identified at 3062, 3023 cm^{-1} and the FT-Raman 3060 cm^{-1} are assigned to C–H stretching vibrations of PDPOSC. In B3LYP and HF methods the value lies in the range of 3064–3026 cm^{-1} and 3033–2997 cm^{-1} (mode no.: 162–155), respectively.

The FT-IR band at 1455 cm^{-1} and the FT-Raman band 1213 cm^{-1} are assigned to C–H in-plane bending vibrations of title molecule. The theoretically computed frequencies for the vibrations showed at 1469, 1466, 1442, 1426, 1419, 1300, 1297, 1214 cm^{-1} and 1503, 1497, 1467, 1455, 1452, 1328, 1323, 1227 cm^{-1} (mode nos.: 131, 130, 125, 121, 120, 109, 108, 100) by B3LYP and HF methods for the C–H in-plane bending, respectively. A result from theoretical wavenumber C–H out-of-plane bending vibrations of the PDPOSC are appeared at 972, 948, 894, 827, 825, 717, 712, 688 cm^{-1} and 995, 981, 922, 859, 844, 740, 726, 700 cm^{-1} (mode nos: 73, 70, 64, 59, 58, 52, 51, 48) by B3LYP and HF methods, respectively. These C–H out-of-plane bending vibrations are finding well supported by the TED values.

C–C vibrations

The ring C=C and C–C stretching vibrations, known as semicircle stretching usually happen in the region 1400–1625 cm^{-1} [30–32]. Hence in the present study, the FT-IR bands at 1578, 1024, 1002 cm^{-1} and the FT-Raman bands at 1580, 1207, 1174, 985, 890 cm^{-1} are assigned to C–C vibrations of PDPOSC and the corresponding calculated values are 1581, 1208, 1179, 1024, 1004, 982, 893 cm^{-1} and 1624, 1207, 1183, 1026, 1014, 1011, 914 cm^{-1} (mode nos.: 135, 99, 96, 81, 78, 76, 63) in B3LYP and HF level theories, respectively.

The bands observed at 616, 512, 439 cm^{-1} in FT-IR and 590, 282 cm^{-1} in FT-Raman spectra have been intended to C–C in-plane and out-of-plane bending modes. The calculated bending modes are found at 611, 589, 504, 440, 287 cm^{-1} (mode nos: 45, 43, 37, 32, 23) in B3LYP/6-311++G(d,p) are assigned to C–C in-plane and out-of-plane bending vibrations, respectively.

In order to investigate the performance and vibrational wavenumbers of title compound, the root mean square value (RMS) was calculated between calculated wavenumbers and observed wavenumbers (Fig. S4a and b). RMS values of wavenumbers were evaluated using the following expression [33].

$$\text{RMS} = \sqrt{\frac{1}{n-1} \sum_i^n (v_i^{\text{calc}} - v_j^{\text{exp}})^2}$$

For IR

$$v_{\text{cal}} = 1.00251 v_{\text{exp}} - 2.10131 \quad (R^2 = 0.99996) \text{ by DFT method}$$

$$v_{\text{cal}} = 0.99739 v_{\text{exp}} + 18.18323 \quad (R^2 = 0.99978) \text{ by HF method}$$

For Raman

$$v_{\text{cal}} = 1.00142 v_{\text{exp}} + 2.64209 \quad (R^2 = 0.99988) \text{ by DFT method}$$

$$v_{\text{cal}} = 0.99427 v_{\text{exp}} + 26.6118 \quad (R^2 = 0.99971) \text{ by HF method}$$

Table 2
Observed and calculated wavenumbers (cm⁻¹) and TED assignments for PDPOSC.

Mode no	Observed frequencies(cm ⁻¹)		Scaled frequencies ^a (cm ⁻¹)		Intensities		TED ≥ 10% ^c
	FT-IR	FT-Raman	B3LYP/6-311++G(d,p)	HF/6-311++G(d,p)	IR	Raman ^b	
1			13	11	0.18	20.96	ΓC1-C2-N12-C3(45)
2			18	15	0.19	100	τC15-C13-C5-N12(21) + τC3-C2-C4-C5(15) + τC1-N12-C4-C5(20)
3			26	25	0.02	59.8	τC26-C24-C1-N12(14) + τC2-C35-C38-c41(32)
4			29	35	0.10	52.53	τC15-C13-C5-N12(24) + τC3-N51-N52-C53(12) + τC3-C2-C4-C5(10) + τC1-N12-C5-C13(18)
5			41	39	0.61	12.63	τC15-C13-C5-N12(10) + τC26-C24-C1-N12(17)
6			47	45	0.93	32.88	βC2-C35-C38(11) + βC35-C38-C41(13) + τC15-C13-C5-N12(11)
7			49	49	0.77	20.48	τN51-N52-C53-N154(16) + τC3-C2-C35-C38(12) + τC2-C35-C38-c41(16)
8			57	57	1.37	15.24	τN51-N52-C53-N154(23) + τC35-C38-C41-C44(14)
9			61	64	0.20	22.33	βC3-N51-N52(10) + τC26-C24-C1-N12(27)
10			70	74	0.36	5.72	τN51-N52-C53-N154(19) + τC1-N12-C5-C13(21) + ΓC1-C24-C26-C25(14)
11			91	99	0.35	18.45	τC3-N51-N52-C53(31) + τC35-C38-C41-C44(18)
12			117	119	0.60	2.45	βC53-N52-N51(12) + βC3-N51-N52(22) + τC35-C38-C41-C44(10)
13			124	124	0.38	1.93	τC38-C41-C44-C47(41) + τC2-C35-C38-c41(12)
14			139	149	1.06	4.72	βC35-C38-C41(13) + τC15-C13-C5-N12(10)
15			158	155	1.04	1.82	βC1-C24-C26(20) + ΓC1-C2-C12-C24(15)
16			164	169	0.58	7.93	τC3-C2-C35-C38(28)
17		165w	169	179	0.21	3.61	βN52-C53-N54(16) + τC27-C25-C31-C29(44)
18			197	201	5.25	8.28	βC53-N52-N51(17)
19			214	212	1.33	4.9	βC5-C13-C15(14) + βC1-C2-C35(12) + βC2-C1-N12(20)
20			230	227	0.51	3.91	βC5-C13-C15(18) + βC1-C2-C35(13)
21			244	239	0.03	0.01	τH48-C47-C44-C41(42) + τH50-C47-C44-C41(38)
22			280	277	0.34	1.28	βC41-C44-C47(14)
23		282w	287	285	3.59	2.69	βC1-C24-C26(11)
24			299	293	8.72	5.65	τC4-C3-N51-N52(21)
25			335	313	41.36	1.14	βC1-C2-C35(14) + ΓN54-H55-C53-H46(16)
26			341	342	33.53	4.73	βC1-C2-C35(13) + ΓN54-H55-C53-H46(16)
27			365	358	133.76	3.85	ΓN54-H55-C53-H46(34)
28			383	386	6.14	3.62	βC41-C44-C47(12) + βC35-C38-C41(18) + ΓC35-C1-C3-C2(12)
29			391	404	28.26	2.44	βC2-C3-C4(15)
30			399	411	0.12	0.12	τC26-C29-C27-C31(30) + τC27-C25-C31-C29(44)
31			403	411	1.80	0.15	τC15-C18-C16-C20(29) + τC16-C14-C20-C18(37)
32		439m	440	444	6.83	0.81	τC15-C18-C16-C20(14) + ΓC3-C13-C15-C14(15)
33			447	453	7.01	0.16	βN52-C53-N54(10) + βC41-C44-C47(12) + βC2-C35-C38(12) + βC38-C41-C44(19)
34			452	466	95.81	1.48	τH57-N52-C53-N54(55) + ΓN54-H55-C53-H46(13)
35			465	471	2.64	0.42	βC13-C5-N12(15) + ΓC5-C13-C15-C14(11)
36			485	490	1.43	0.85	βC2-C3-N51(19)
37		512m	504	512	1.43	1.1	βC14-C13-C15(18)
38			518	529	9.64	0.95	ΓC1-C24-C26-C25(14)
39			533	543	25.86	1.89	τH57-N52-C53-N54(19) + ΓH55-N54-C53-N52(41)
40			549	558	35.72	0.6	ΓH55-N54-C53-N52(14)
41			571	587	24.74	3.36	βN52-C53-N54(12) + ΓN12-C1-C5-H11(41) + ΓN51-C2-C4-C3(20)
42			579	597	17.39	1.96	βN52-C53-N54(16) + ΓN12-C1-C5-H11(13)
43		590w	589	610	29.22	1.24	βC2-C3-N51(22)
44			610	613	0.07	2.03	βC26-C29-C31(46) + βC25-C27-C31(21)
45		616w	611	614	0.29	3.24	βC15-C18-C20(46) + βC14-C16-C20(22)
46			625	634	8.30	2.51	βC2-C3-N51(10) + βC27-C31-C29(12)
47		676w	670	697	42.98	0.56	ΓN12-C1-C5-H11(31)
48			688	700	42.57	0.25	ΓH17-C14-C16-C20(11) + τC13-C15-C20-C18(43) + τC15-C18-C16-C20(14) + τC16-C14-C20-C18(20)
49			689	704	30.59	0.47	τC24-C26-C31-C29(49) + τC26-C29-C27-C31(16) + τC27-C25-C31-C29(18)
50		697s	708	709	6.76	0.26	τH36-C35-C38-H39(10) + τH42-C41-C44-C47(13) + τH43-C41-C44-C47(15) + τH43-C41-C44-H45(27)
51			712	726	7.42	2.32	vC5-C13(11) + βC16-C20-C18(19) + ΓC15-C13-C18-H19(11)
52			717	740	72.70	1.09	ΓC20-C16-C18-H23(11) + βC2-C3-C4(16)
53			731	750	21.48	0.11	ΓO58-H52-N54-C53(88)
54			733	771	1.70	1.63	τH36-C35-C38-H39(20)
55		758s	750	780	16.58	0.34	ΓC26-C24-C29-C30(17) + ΓC26-C24-C29-H30(18) + τH30-C26-C29-H33(13) + ΓC1-C24-C26-C25(12)
56			776	789	5.40	4.92	βC27-C31-C29(12)
57			807	820	5.71	2.04	τH48-C47-C44-C41(10)

(continued on next page)

Table 2 (continued)

Mode no	Observed frequencies(cm^{-1})		Scaled frequencies ^a (cm^{-1})		Intensities		TED $\geq 10\%$ ^c
	FT-IR	FT-Raman	B3LYP/6-311++G(d,p)	HF/6-311++G(d,p)	IR	Raman ^b	
58			825	844	0.29	0.24	$\Gamma\text{C}26\text{-C}24\text{-C}29\text{-H}30(46) + \Gamma\text{H}32\text{-C}27\text{-C}25\text{-C}24(46)$
59			827	859	0.34	0.23	$\Gamma\text{H}17\text{-C}14\text{-C}16\text{-C}20(34) + \Gamma\text{C}15\text{-C}13\text{-C}18\text{-H}19(45)$
60			836	861	10.10	0.28	$\nu\text{C}2\text{-C}3(17)$
61			860	866	1.95	1.43	$\nu\text{C}44\text{-C}47(17) + \nu\text{C}41\text{-C}44(20) + \beta\text{H}48\text{-C}47\text{-C}44(18)$
62			880	900	5.38	2.44	$\tau\text{H}30\text{-C}26\text{-C}29\text{-H}33(13) + \tau\text{H}33\text{-C}29\text{-C}31\text{-H}34(10) + \tau\text{H}28\text{-C}25\text{-C}27\text{-H}32(11)$
63		890w	893	914	4.45	4.25	$\nu\text{C}4\text{-C}5(10)$
64			894	922	0.61	0.77	$\Gamma\text{H}17\text{-C}14\text{-C}16\text{-C}20(11) + \Gamma\text{C}20\text{-C}16\text{-C}18\text{-H}23(10)$
65			901	931	8.91	1.04	$\nu\text{C}4\text{-C}5(28)$
66			907	938	4.38	0.61	$\Gamma\text{H}17\text{-C}14\text{-C}16\text{-C}20(10) + \Gamma\text{C}20\text{-C}16\text{-C}18\text{-H}23(10)$
67			928	955	26.15	1.81	
68			942	962	12.65	0.74	$\nu\text{N}54\text{-C}53(38) + \nu\text{N}52\text{-C}53(17)$
69	945m		944	980	0.05	0.06	$\tau\text{H}30\text{-C}26\text{-C}29\text{-H}33(43) + \tau\text{H}28\text{-C}25\text{-C}27\text{-H}32(43)$
70			948	981	1.19	0.03	$\Gamma\text{H}17\text{-C}14\text{-C}16\text{-C}20(11) + \tau\text{H}19\text{-C}15\text{-C}18\text{-H}22(53) + \Gamma\text{C}20\text{-C}16\text{-C}18\text{-H}23(19)$
71			965	989	1.31	0.51	$\tau\text{H}33\text{-C}29\text{-C}31\text{-H}34(47)$
72			969	994	4.66	1.44	$\tau\text{H}17\text{-C}14\text{-C}16\text{-H}21(10) + \tau\text{H}33\text{-C}29\text{-C}31\text{-H}34(11)$
73			972	995	1.25	0.6	$\tau\text{H}17\text{-C}14\text{-C}16\text{-H}21(57) + \Gamma\text{C}20\text{-C}16\text{-C}18\text{-H}23(13)$
74			978	997	0.21	10.65	$\beta\text{C}15\text{-C}18\text{-C}20(20) + \beta\text{C}16\text{-C}20\text{-C}18(19) + \beta\text{C}14\text{-C}16\text{-C}20(25)$
75			978	1007	2.67	7.37	$\beta\text{C}26\text{-C}29\text{-C}31(18) + \beta\text{C}27\text{-C}31\text{-C}29(18) + \beta\text{C}25\text{-C}27\text{-C}31(25)$
76		985w	982	1011	5.84	0.46	$\nu\text{C}44\text{-C}47(34) + \nu\text{C}38\text{-C}41(22)$
77			991	1014	2.94	1.72	$\nu\text{N}12\text{-C}1(13)$
78	1002w		1004	1014	2.74	1.46	$\nu\text{C}35\text{-C}38(36)$
79			1011	1017	2.79	4.55	$\nu\text{C}29\text{-C}31(19) + \nu\text{C}27\text{-C}31(24) + \beta\text{H}33\text{-C}29\text{-C}31(10) + \beta\text{C}25\text{-C}27\text{-C}31(10)$
80			1012	1024	12.51	4.31	$\nu\text{C}18\text{-C}20(17) + \nu\text{C}16\text{-C}20(22)$
81	1024m		1024	1026	0.67	2.37	$\nu\text{C}44\text{-C}47(21) + \nu\text{C}38\text{-C}41(33) + \nu\text{C}41\text{-C}44(33)$
82			1036	1058	15.85	1.4	$\nu\text{C}35\text{-C}38(10) + \nu\text{C}2\text{-C}35(25)$
83			1054	1061	14.03	0.35	$\nu\text{C}15\text{-C}18(12) + \nu\text{N}12\text{-C}5(11)$
84			1060	1065	24.95	0.26	$\nu\text{C}35\text{-C}38(16) + \beta\text{C}25\text{-C}27\text{-C}31(21)$
85			1069	1082	13.66	0.75	$\nu\text{C}2\text{-C}35(11) + \beta\text{H}55\text{-N}54\text{-C}53(21)$
86			1080	1083	25.57	1.47	$\nu\text{N}12\text{-C}5(13)$
87	1092m		1084	1094	13.36	0.13	$\nu\text{C}4\text{-C}5(18) + \beta\text{C}16\text{-C}20\text{-C}18(11)$
88			1102	1099	30.29	0.92	$\nu\text{N}51\text{-N}52(23)$
89			1107	1112	23.87	0.9	
90			1131	1130	9.84	3.24	$\nu\text{C}5\text{-C}13(12) + \beta\text{H}8\text{-C}4\text{-C}3(15)$
91			1135	1134	1.86	0.76	$\beta\text{H}21\text{-C}16\text{-C}20(26) + \beta\text{H}22\text{-C}18\text{-C}20(11) + \beta\text{H}22\text{-C}18\text{-C}20(33)$
92			1137	1152	0.06	0.8	$\beta\text{H}32\text{-C}27\text{-C}25(18) + \beta\text{H}33\text{-C}29\text{-C}31(21) + \beta\text{H}33\text{-C}29\text{-C}31(37)$
93	1142w		1156	1171	10.86	1.26	$\beta\text{H}17\text{-C}14\text{-C}13(17) + \beta\text{H}19\text{-C}15\text{-C}18(21) + \beta\text{H}21\text{-C}16\text{-C}20(10) + \beta\text{H}22\text{-C}18\text{-C}20(24)$
94			1159	1173	1.02	0.89	$\beta\text{H}30\text{-C}26\text{-C}29(19) + \beta\text{H}32\text{-C}27\text{-C}25(19) + \beta\text{H}33\text{-C}29\text{-C}31(17) + \beta\text{H}28\text{-C}25\text{-C}27(20)$
95			1167	1183	53.80	7.28	$\beta\text{H}28\text{-C}25\text{-C}27(14)$
96		1174w	1179	1183	33.12	2.81	$\nu\text{C}1\text{-C}24(13)$
97			1180	1201	2.80	2.7	$\beta\text{C}4\text{-C}5\text{-N}12(10) + \tau\text{H}9\text{-C}4\text{-C}3\text{-C}2(29) + \Gamma\text{C}5\text{-C}4\text{-C}13\text{-H}10(12)$
98			1192	1203	9.96	2.62	$\beta\text{H}8\text{-C}4\text{-C}3(15) + \beta\text{H}10\text{-C}5\text{-C}13(35)$
99		1207m	1208	1207	33.30	2.31	$\nu\text{C}1\text{-C}24(10)$
100		1213m	1214	1227	1.12	0.55	$\beta\text{H}17\text{-C}14\text{-C}13(11) + \beta\text{H}19\text{-C}15\text{-C}18(13) + \beta\text{H}30\text{-C}26\text{-C}29(15)$
101			1220	1238	5.88	0.3	$\beta\text{H}28\text{-C}25\text{-C}27(16) + \tau\text{H}36\text{-C}35\text{-C}38\text{-H}39(14)$
102			1239	1245	9.32	1.77	$\nu\text{C}24\text{-C}26(11)$
103			1261	1273	4.36	0.57	$\beta\text{H}36\text{-C}35\text{-C}38(10) + \beta\text{H}45\text{-C}44\text{-C}47(11) + \tau\text{H}42\text{-C}41\text{-C}44\text{-H}46(22)$
104			1269	1285	4.66	1.08	$\nu\text{C}16\text{-C}20(13) + \nu\text{C}13\text{-C}15(22)$
105			1277	1297	8.86	0.75	$\beta\text{H}45\text{-C}44\text{-C}47(26)$
106			1285	1304	0.84	4.02	$\beta\text{H}39\text{-C}38\text{-C}35(12) + \beta\text{H}42\text{-C}41\text{-C}44(40) + \beta\text{H}45\text{-C}44\text{-C}47(12)$
107			1291	1308	5.30	1.21	$\beta\text{H}10\text{-C}5\text{-C}13(13)$
108			1297	1323	1.14	0.55	$\nu\text{C}25\text{-C}27(10) + \beta\text{H}17\text{-C}14\text{-C}13(10) + \beta\text{H}19\text{-C}15\text{-C}18(10) + \beta\text{H}30\text{-C}26\text{-C}29(10) + \beta\text{H}28\text{-C}25\text{-C}27(12)$
109			1300	1328	4.51	1.17	$\beta\text{H}17\text{-C}14\text{-C}13(11) + \beta\text{H}19\text{-C}15\text{-C}18(12)$
110			1304	1336	0.11	1.37	$\beta\text{H}36\text{-C}35\text{-C}38(23) + \beta\text{H}39\text{-C}38\text{-C}35(19)$
111			1306	1348	18.07	1.25	$\beta\text{H}10\text{-C}5\text{-C}13(13) + \tau\text{H}7\text{-C}1\text{-C}24\text{-C}26(24) + \tau\text{H}8\text{-C}4\text{-C}3\text{-C}2(12)$
112			1318	1350	11.55	1.59	$\Gamma\text{C}5\text{-C}4\text{-C}13\text{-H}10(22)$
113			1325	1362	26.76	1.43	$\tau\text{H}7\text{-C}1\text{-C}24\text{-C}26(12) + \Gamma\text{C}2\text{-C}1\text{-C}3\text{-H}6(34)$
114		1330w	1334	1375	15.28	0.46	$\beta\text{H}7\text{-C}1\text{-C}24(26) + \Gamma\text{C}5\text{-C}4\text{-C}13\text{-H}10(28)$
115			1346	1388	2.34	0.09	$\tau\text{H}36\text{-C}35\text{-C}38\text{-H}40(12) + \tau\text{H}42\text{-C}41\text{-C}44\text{-C}47(25) + \tau\text{H}43\text{-C}41\text{-C}44\text{-C}47(21)$

Table 2 (continued)

Mode no	Observed frequencies(cm^{-1})		Scaled frequencies ^a (cm^{-1})		Intensities		TED $\geq 10\%$ ^c
	FT-IR	FT-Raman	B3LYP/6-311++G(d,p)	HF/6-311++G(d,p)	IR	Raman ^b	
116			1350	1396	67.36	0.63	Γ C2-C1-C3-H6 (14) + τ H36-C35-C38-H41(10) + τ H37-C35-C38-H41(11)
117	1353m		1356	1400	169.56	0.26	ν N54-C53 (14) + ν N52-C53 (13) + β H55-N54-H56 (10) + β H55-N54-C53(12) + β N52-N53-O58(10)
118			1360	1407	9.71	0.14	β H48-C47-C44(34) + β H49-C47-C50(51)
119			1403	1442	148.13	1.11	ν N52-C53 (12) + β H57-N52-N51(52)
120			1419	1452	6.81	0.36	ν C15-C18 (12) + ν C14-C16 (12) + β H21-C16-C20(12) + β H22-C18-C20(11) + β H23-C20-C16(24)
121			1426	1455	2.00	0.43	ν C26-C29(11) + ν C25-C27(10) + β H33-C29-C31(10) + β H34-C31-C29(22)
122			1430	1458	9.01	3.1	β H8-C4-H9(27) + β H42-C41-H43(36) + β H45-C44-H46(22)
123			1431	1461	24.85	1.75	β H8-C4-H9(45) + β H42-C41-H43(19) + β H45-C44-H46(10)
124			1434	1461	0.40	0.16	β H39-C38-H40(40) + β H45-C45-H46(24)
125			1442	1467	4.33	2.3	β H11-N12-C1(15) + β H36-C35-H37(12) + β H39-C38-H40(22) + β H49-C47-H50(11)
126			1443	1472	5.69	1.77	β H48-C47-H49(63) + τ H49-C47-C44-C41(14)+) + τ H50-C47-C44-C41(11)
127			1444	1475	16.64	0.4	β H11-N12-C1(47)
128			1452	1485	2.22	0.32	β H36-C35-H37(19) + β H45-C44-H46(31) + β H49-C47-H50(14)
129			1461	1488	7.61	0.31	β H36-C35-H37(45) + β H39-C38-H40(14) + β H42-C41-H43(12)
130			1466	1497	18.15	0.15	β H17-C14-C13(13) + β H19-C15-C18(19) + β H21-C16-C20(17) + β H22-C18-C20(16)
131	1455s		1469	1503	7.39	0.17	β H30-C26-C29(15) + β H32-C27-C25(19) + β H33-C29-C31(17) + β H28-C25-C27(18)
132		1522m	1524	1544	298.30	2.58	β H55-N54-H56(84)
133			1560	1598	0.74	1.08	ν C18-C20(31) + ν C13-C15(26)+) + β C14-C16-C20(26)
134			1563	1601	1.99	0.8	ν C29-C31(19) + ν C24-C26(27) + β C25-C27-C31(11)
135	1578m	1580m	1581	1624	7.98	4.08	ν C15-C18(19) + ν C14-C16(16) + ν C16-C20(10) + β C14-C13-C15(11)
136	1649w	1600m	1650	1655	2.73	5.27	ν N51-C3(78) + ν N54-C53(10)
137	1691s	1685s	1695	1713	12.46	28.29	ν O58-C53(72)
138			1733	1767	464.72	2.44	ν C26-C29(17) + ν C25-C27(18) + ν C25-C24(12)
139			2870	2840	1.63	2.1	ν C2-H6(72) + ν C35-H36(26)
140			2877	2841	3.18	0.56	ν C2-H6(19) + ν C35-H36(43) + ν C38-H39(26)
141			2879	2845	4.25	4.96	ν C41-H42(43) + ν C38-H39(27)
142			2887	2849	1.06	0.93	ν C35-H36(13) + ν C38-H39(27) + ν C44-H45(24) + ν C44-H46(24)
143			2892	2855	55.74	2.27	ν C38-H39(20) + ν C38-H39(27) + ν C44-H46(32)
144	2856m		2894	2856	13.76	2	ν C4-H8(18) + ν C5-H10(71)
145			2902	2861	12.13	4.58	ν C41-H42(17) + ν C41-H43(11) + ν C44-H45(19) + ν C47-H49(10) + ν C47-H50(19)
146			2902	2866	41.53	3.35	ν C41-H42(15) + ν C44-H45(14) + ν C47-H48(18) + ν C47-H49(26) + ν C47-H50(18)
147			2907	2880	52.93	11.02	ν C4-H8(65) + ν C5-H10(23)
148			2912	2881	47.59	0.26	ν C1-H7(84)
149	2927m	2930m	2927	2939	35.22	0.38	ν C41-H42(21) + ν C41-H43(16) + ν C44-H45(26) + ν C44-H46(24)
150			2942	2940	7.22	2.57	ν C35-H37(80) + ν C38-H40(10)
151	2955w		2960	2965	49.39	1.23	ν C47-H49(45) + ν C47-H50(45)
152			2965	2970	43.39	3.75	ν C47-H48(72) + ν C47-H49(13) + ν C47-H50(13)
153			2974	2975	41.26	0.65	ν C38-H40(80)
154			2996	2980	22.44	2.33	ν C4-H9(93)
155	3023m		3026	2997	11.11	0.96	ν C27-H32(13) + ν C25-H28(84)
156			3035	3001	0.93	1.38	ν C16-H21(26) + ν C18-H22(36) + ν C20-H23(31)
157			3037	3003	2.31	1.3	ν C27-H32(53) + ν C29-H33(31) + ν C31-H34(11)
158			3043	3011	9.91	3.73	ν C27-H32(10) + ν C16-H21(49) + ν C18-H22(11)
159			3046	3013	6.44	3.07	ν C26-H30(27) + ν C27-H32(24) + ν C31-H34(40)
160			3054	3022	25.37	1.97	ν C26-H30(15) + ν C27-H32(41) + ν C29-H33(38)
161			3056	3026	30.91	2.18	ν C27-H32(38) + ν C16-H21(13) + ν C20-H23(45)
162	3062m	3060s	3064	3033	20.58	5.37	ν C27-H32(20) + ν C18-H22(26) + ν C20-H23(21)
163			3065	3048	17.56	10.36	ν C27-H32(20) + ν C29-H33(28) + ν C31-H34(45)
164	3196m		3198	3211	5.81	4.36	ν C14-H17(87)
165			3421	3433	2.16	1.68	ν N12-H11(99)
166			3448	3477	33.49	1.61	ν N54-H55(35) + ν N54-H56(64)
167	3461s		3453	3509	18.94	3.13	ν N55-H57(95)
168			3579	3599	82.01	1.09	ν N54-H55(65) + ν N54-H56(34)

s – strong, m – medium, w – weak.

a – Scale factor: 0.9608-B3LYP/6-311++G(d,p),0.9051-(HF/6-311++G(d,p).

b – Relative Raman intensities calculated by equation and normalized to 100.

c – ν : stretching; β – in-plane bending; Γ – out-of-plane bending; τ – torsion; TED: Total energy distribution.

The RMS error of the observed Raman bands, IR bands and the scaled wavenumbers are found to be 21.56, 22.24 (HF) and 19.98, 9.92 (B3LYP), respectively. It clearly shows that the calculated frequencies by B3LYP/6-311++G(d,p) method is tally with experimental frequencies.

NBO analysis

A useful aspect of the NBO method is that it gives information about the interactions in both filled and virtual orbital spaces that could enhance the analysis of intra- and inter molecular interactions. The second-order Fock matrix was carried out to evaluate the donor–acceptor interactions in the NBO analysis [34]. The interactions result in a loss of occupancy from the localized NBO of the idealized Lewis structure into an empty non-Lewis orbital. For each donor (i) and acceptor (j), the stabilization energy $E^{(2)}$ associated with the delocalization $i \rightarrow j$ is estimated as

$$E^{(2)} = \Delta E_{ij} = q_i \frac{F(i,j)^2}{\epsilon_j - \epsilon_i}$$

Where q_i is the donor orbital occupancy, ϵ_i and ϵ_j are diagonal elements and $F(i, j)$ is the off diagonal NBO Fock matrix element. Natural bond orbital analysis provides an efficient method for studying intra- and intermolecular binding and interaction among bonds, and also provides a convenient basis for investigating charge transfer or conjugative interaction in molecular systems. Some electron donor orbital, acceptor orbital and the interacting stabilization energy resulted from the second-order micro-disturbance theory are reported [35,36]. The larger the $E^{(2)}$ value, the more interaction between electron donors and electron acceptors, i.e. the more donating tendency from electron donors to electron acceptors and the greater the extent of conjugation of the whole system. NBO analysis has been performed on the molecule at the DFT/B3LYP level using 6-311++G(d,p) basis set in order to elucidate the intramolecular, re-hybridization and delocalization of electron density within the molecule.

The second-order perturbation theory analysis of Fock matrix in NBO basis shows strong intramolecular hyperconjugative interactions of π electrons. The intra-molecular hyperconjugative interactions is due to the overlap between π (C–C) and π^* (C–C) orbitals, which results in intramolecular charge transfer appearing in the molecular system [37]. It is evident from our calculation that the $E^{(2)}$ energy of π C29–C31 versus π^* C25–C27 is about 88.16 kJ/mol, and their electron densities are 1.66 and 0.33e, respectively. Similarly, the π – π^* interaction of C13–C14 \rightarrow C16–C20, C15–C18 \rightarrow C13–C14, C16–C20 \rightarrow C15–C18, C24–C26 \rightarrow C29–C31,

C25–C27 \rightarrow C24–C26 bonds revealed that the maximum hyperconjugative interaction energy $E^{(2)}$ in both the phenyl rings are having lesser electron densities than σ bonds. The above interactions are observed as an increase in electron density (ED) in C–C anti bonding orbital that weakens the respective donor bonds. The intramolecular hyperconjugative interactions are formed by the orbital overlap between $n(N)$ and $\pi^*(C-N)$ bond and $n(N)$ and $\pi^*(N-O)$ bond orbital which results in ICT causing stabilization of the system. The strong intra-molecular hyperconjugative interaction of C3–N51 from N52 of $n1(N52) \rightarrow C3-N51$ which increases ED (0.19e) and that weakens the respective bonds leading to stabilization of 121.29 kJ mol⁻¹. The higher ED value with lower $E^{(2)}$ energy which causes lesser interaction and hence it shifts the vibrational frequencies from the actual frequency range. It is evident that C3–N51 (1.956 e) bond stretching vibration appears at 1650 and 1655 cm⁻¹ by B3LYP and HF, respectively (mode no. 136). These vibrations are higher from the normal C–N bond stretching (1300 cm⁻¹) [38]. Also there is another hyper conjugative interaction observed in $n1(N54) \rightarrow \pi^* C3-O58$ bond, having ED (0.30e) with a stabilization of 118.62 kJ mol⁻¹. These interactions are observed as an increase in electron density (ED) in C–N and C–O anti-bonding orbitals that weakens the respective bonds. The electron density (ED) is transferred from the $n(N)$ to the anti-bonding π^* orbital of the C–N and C–O bonds. The $n2(O58)$ orbital interacts with N52–C53 and C53–N54 antibonding orbital that leads to give stabilization energy of 103.64 and 93.93 kJ mol⁻¹, respectively. Electron density and delocalization energy of PDPOSC are given in Table 3.

Mulliken charge analysis

Charge distribution on a molecule has a significant influence of the vibrational spectra. The Mulliken population analysis of PDPOSC was done using B3LYP/6-311++G(d,p) basis set and the data are listed in Table S2. The Mulliken atomic charges are shown in Fig. 3.

The more positive charge on C53 (0.4869) carbon atom is due to the highly electronegative nitrogen and oxygen attached to that carbon atom. This is caused by the –I effect of nitrogen and oxygen atoms. The high negative charge at O58 (–0.3947) and a positive charge at C53, suggest that charge delocalization occurs in the entire molecule.

Molecular electrostatic potential

The molecular electrostatic potential (MEP) are related to the electron density and may be a helpful descriptor in understanding

Table 3
Second order perturbation theory analysis of Fock matrix in NBO for PDPOSC.

Type	Donor (i)	ED/e	Acceptor (j)	ED/e	$E^{(2)}$ (kJ/mol)	Ej-Ei (a.u.)	Fi,j (a.u.)
π – π^*	C13–C14	1.65059	C16–C20	0.01720	88.07	0.28	0.069
π – σ^*	C3–N51	1.95584	C1 – C2	0.05332	8.12	0.66	0.032
π – π^*	C15–C18	1.67350	C13–C14	0.34235	85.40	0.29	0.069
π – π^*	C16–C20	1.97911	C15–C18	0.33139	87.65	0.28	0.069
π – π^*	C24–C26	1.65545	C29–C31	0.32464	88.12	0.28	0.069
π – π^*	C25–C27	1.67636	C24–C26	0.33810	87.70	0.29	0.070
π – π^*	C29–C31	1.66446	C24–C26	0.33810	82.59	0.29	0.067
π – π^*			C25–C27	0.32731	88.16	0.28	0.069
n – σ^*	LP (1) N12	1.90811	C1–C2	0.05332	36.78	0.62	0.066
n – σ^*			C4–C5	0.03932	32.84	0.63	0.064
n – σ^*	LP (1) N51	1.91529	C2–C3	0.04683	58.74	0.77	0.093
n – σ^*			N52–H57	0.03047	36.07	0.78	0.074
n – π^*	LP (1) N52	1.71725	C3–N51	0.19208	121.29	0.29	0.084
n – π^*			C53–O58	0.29940	112.68	0.41	0.094
n – π^*	LP (1) N54	1.79024	C53–O58	0.29940	118.62	0.41	0.098
n – σ^*	LP (2) O58	1.84819	N52–C53	0.08122	103.64	0.65	0.116
n – σ^*			C53–N54	0.06546	93.93	0.69	0.114

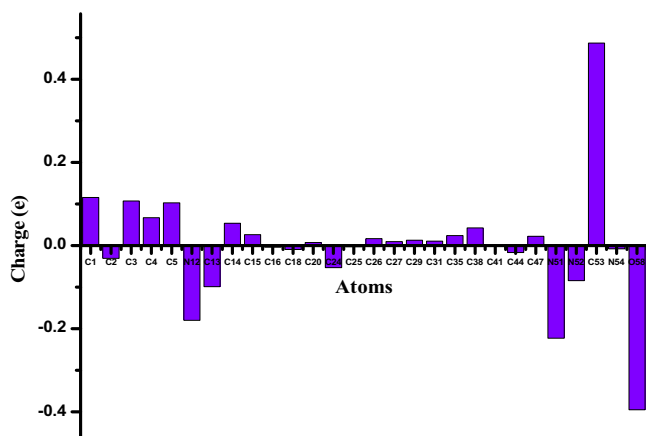


Fig. 3. The atomic charge plot of PDPOSC.

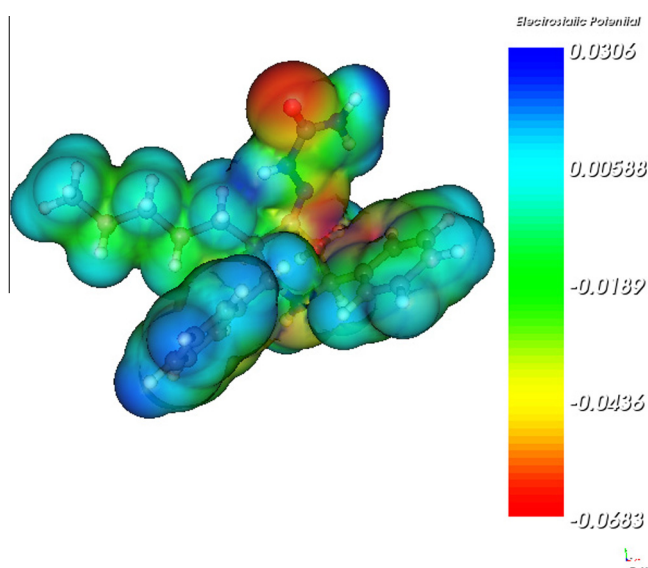


Fig. 4. Molecular electrostatic potential of PDPOSC.

sites for electrophilic and nucleophilic attacks and also hydrogen-bonding interactions [39–41]. To predict reactive sites for electrophilic and nucleophilic attack for the title molecule, MEP was calculated by applying the DFT/B3LYP method and 6-311++G(d,p) basis set for the optimized geometry. The negative (red) regions of MEP were associated with electrophilic reactivity and the positive (blue) regions to nucleophilic reactivity as shown in Fig. 4.

The MEP of the N atom (N51) and oxygen (O58) of PDPOSC is shown by red and yellow colors appearing below and on top of molecular plane of N51 and O58 atoms and that represent the high electron region. Potential will increase with the order red < orange and the colour code of the map is within the range between -0.0683 a.u. (deepest red) and 0.0306 a.u. (deepest blue), where blue indicates the strongest attraction and red indicates the strongest repulsion within the molecule.

Analysis of frontier molecular orbitals

TD-DFT has been most widely used to compute the energy of molecules with high accuracy and low computational cost. Molecular orbitals and their properties like energy are very useful to the physicists and chemists and their frontier electron density is used for predicting the most reactive position in pi-electron system

and also to explain several types of reactions in conjugated systems [42]. The total energy, energy gap and dipole moment affect the stability of a molecule. The conjugated molecules are characterized by a highest occupied molecular orbital–lowest unoccupied molecular orbital (HOMO–LUMO) separation, which is the result of a significant degree of intermolecular charge transfer (ICT) from the end-capping electron-donor to the electron deficient acceptor group through pi-conjugated path. The energy gap between the HOMO and LUMO molecular orbitals is a critical parameter in determining molecular electrical transport properties because it is a measure of electron conductivity. So as to evaluate energetic behavior of the title compound, we have carried out calculations in gas, methanol and chloroform solvents. According to the investigation of FMO energy levels of the title compound, we noticed that the corresponding electronic transfers happened between HOMO and LUMO + 1 and HOMO – LUMO. 3D plots of the HOMO and LUMO orbitals computed at TD-B3LYP/6-311++G(d,p) level PDPOSC molecule, in gas phase, methanol and chloroform are illustrated in Fig. 5. The positive phase is red and the negative one is green. It is clear from the figure that, the HOMO lying at -5.901 , -5.906 and -5.870 eV in methanol, chloroform and gas phase, respectively and it is located mainly over the piperidine ring and semicarbazone group. LUMO lying at -0.767 , -0.593 and -0.547 eV in methanol, chloroform and gas phase, respectively and it is located in phenyl group attached at C1 position of piperidone moiety. The value of energy gap between the HOMO–LUMO is 5.134, 5.313 and 5.320 eV in methanol, chloroform and gas phase, respectively. The energy gap of HOMO–LUMO explains the eventual charge transfer interactions that take place within the molecule. Furthermore, in going from solvent phase to gas phase, the increasing value of the energy gap makes the molecule more stable [43].

The dipole moment is another important electronic property in a molecule. For example higher the dipole moment, the stronger will be the intermolecular interactions. The calculated dipole moment values are given in Table S3. Based on predicted dipole moment values, it is found that, in going to the solvent phase from (6.214 D in methanol) from gas phase (4.540 D), the dipole moment value decreases (Table S3) which indicates that polarity of solvent influences the dipole moment of the studied molecule. The values of electronegativity, chemical hardness, softness and electrophilicity index are also given in Table S3.

Ultraviolet spectral analysis

The electronic spectra of the title compound in methanol and chloroform solvents were recorded and shown in Fig. S5. There is no absorption band around 400 and 1000 nm. The absence of absorption in the visible region in the case semicarbazone makes them suitable candidate for NLO property. [44,45]. As seen from Fig. S5, electronic absorption spectra showed two bands at 269.5 and 252.5 nm for chloroform at 284.0 and 245.0 nm for methanol. Electronic absorption spectra were calculated using the TD-DFT method based on the B3LYP/6-311++G(d,p) level optimized structure in gas phase. The calculated results are listed in Table 4 along with the experimental absorption spectral data. For TD-DFT calculations, the theoretical absorption bands are predicted at 272.01, 262.40 and 253.85 nm in gas phase, at 267.87, 255.69 and 251.82 nm in chloroform and 267.90, 255.65 and 252.95 nm in methanol. The band at 284.5 nm (Chloroform) and 269.5 nm (methanol) are assigned to $n-\pi^*$ transition.

The band at 252.5 nm (Chloroform) and 245.0 nm (methanol) are assigned to $\pi-\pi^*$ transition. The solvent in which the absorbing species is dissolved also has an effect on the spectrum of the species. Peaks resulting from $n-\pi^*$ transitions are shifted to shorter

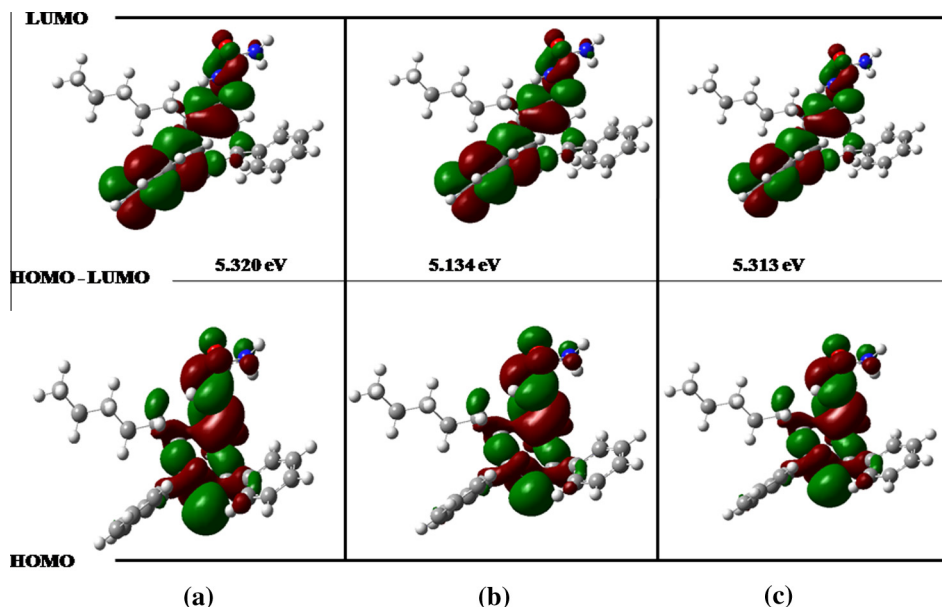


Fig. 5. Molecular orbitals and energies for the HOMO and LUMO in (a) gas phase, (b) methanol and (c) chloroform.

Table 4

Experimental absorption bands and TD-DFT calculated energy transition, visible absorption wavelengths (λ) and oscillator strengths (f) for PDPOSC.

Gas phase			Chloroform			Expt.	Methanol			Expt.	Assignment	Gas phase Major contribution ^a
Energy transition (eV)	λ (nm)	f	Energy transition (eV)	λ (nm)	f		Energy transition (eV)	λ (nm)	f			
4.5581	272.01	0.0678	4.6285	267.87	0.1245	269.50	4.6280	267.90	0.1161	284.0	$n-\pi^*$	H \rightarrow L (93%)
4.7251	262.40	0.0140	4.8490	255.69	0.0108	252.5	4.8497	255.65	0.0066	245.0	$\pi \rightarrow \pi^*$	H \rightarrow L + 1 (95%)
4.8841	253.85	0.0138	4.9235	251.82	0.0043		4.9016	252.95	0.0020		$\pi \rightarrow \pi^*$	H \rightarrow L + 2 (94%)

^aH: HOMO, L: LUMO.

wavelengths (blue shift) with increasing solvent polarity. This emerges from increased solvation of the lone pair, which brings down the energy of the n orbital. Normally (but not always), the reverse (i.e. red shift) is seen for $\pi-\pi^*$ transitions. This is brought about by attractive polarisation forces between the solvent and absorber, which decrease the energy levels of both the excited and unexcited states. This effect is greater for the excited state, and so the energy difference between the excited and unexcited states are slightly reduced – resulting in a small red shift. This effect also influences $n-\pi^*$ transitions but is overshadowed by the blue shift resulting from solvation of lone pairs. The main contributions of the transitions were designated with the help of SWizard program [46]. In gas phase, the maximum absorption wavelength corresponds to the electronic transition from the HOMO–LUMO with 93% contribution, the transition on HOMO–LUMO + 1 with 95% and the transition HOMO–LUMO + 2 with 94%.

Non-linear optical effects

Non-linear optical (NLO) effects arise from the interactions of electromagnetic fields in various media to produce new fields altered in phase, frequency, amplitude or other propagation characteristics from the incident fields [47]. NLO is at the forefront of current research because of its importance in providing the key functions of frequency shifting, optical modulation, optical switching, optical logic and optical memory for the emerging technologies in areas such as telecommunications, signal processing and optical interconnections [48–50]. The complete equations for

Table 5

The mean polarizability (esu), anisotropy polarizability (esu) and first hyperpolarizability (esu) of PDPOSC.

NLO behavior	B3LYP 6-311++G(d,p)	HF 6-311++G(d,p)
Mean polarizability (α)	24.995×10^{-24}	25.193×10^{-24}
Anisotropy of the polarizability ($\Delta\alpha$)	4.40614×10^{-24}	4.80778×10^{-24}
First order polarizability (β_o)	6.5662×10^{-31}	6.68409×10^{-31}

calculating the magnitude of the total static dipole moment (μ), mean polarizability (α_{tot}) and mean hyperpolarizability (β_o), using the x, y, z components from Gaussian 03W output are as follows:

$$\mu = (\mu_x^2 + \mu_y^2 + \mu_z^2)^{1/2}$$

$$\alpha_{tot} = \frac{1}{3}(\alpha_{xx} + \alpha_{yy} + \alpha_{zz})$$

$$\Delta\alpha = \frac{1}{\sqrt{2}}[(\alpha_{xx} - \alpha_{yy})^2 + (\alpha_{yy} - \alpha_{zz})^2 + (\alpha_{zz} - \alpha_{xx})^2 + 6(\alpha_{xy}^2 + \alpha_{yz}^2 + \alpha_{xz}^2)]^{1/2}$$

$$\beta_o = [(\beta_{xxx} + \beta_{xyy} + \beta_{xzz})^2 + (\beta_{yyy} + \beta_{yzz} + \beta_{yxx})^2 + (\beta_{zzz} + \beta_{zxx} + \beta_{zyy})^2]^{1/2}$$

The linear polarizability (α_{tot}) and first-order hyperpolarizability (β_{tot}) of the title compound were calculated by the B3LYP and HF levels using 6-311++G(d,p) basis set. The calculated mean linear

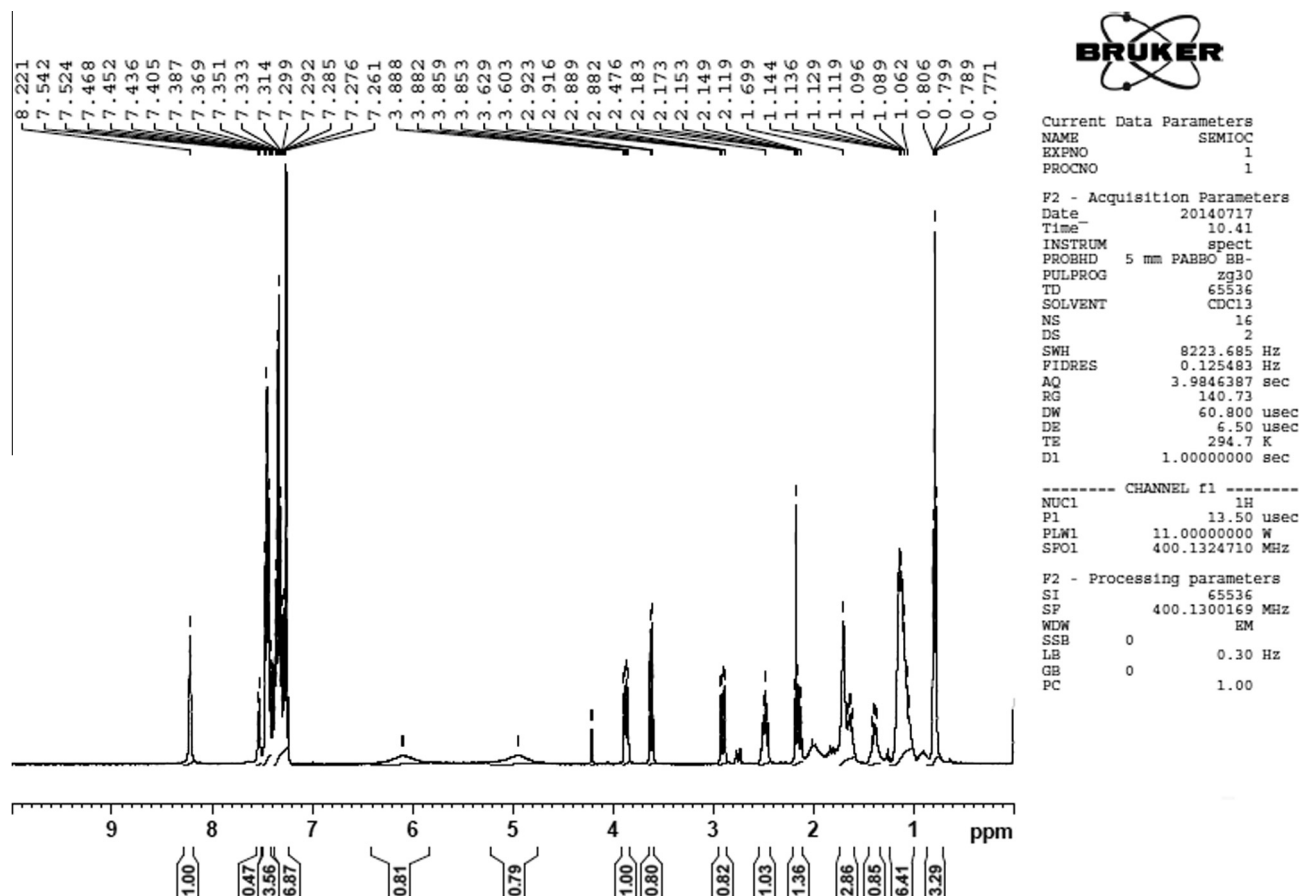
Table 6The experimental and calculated ^1H and ^{13}C NMR chemical shifts (ppm) of PDPOSC.

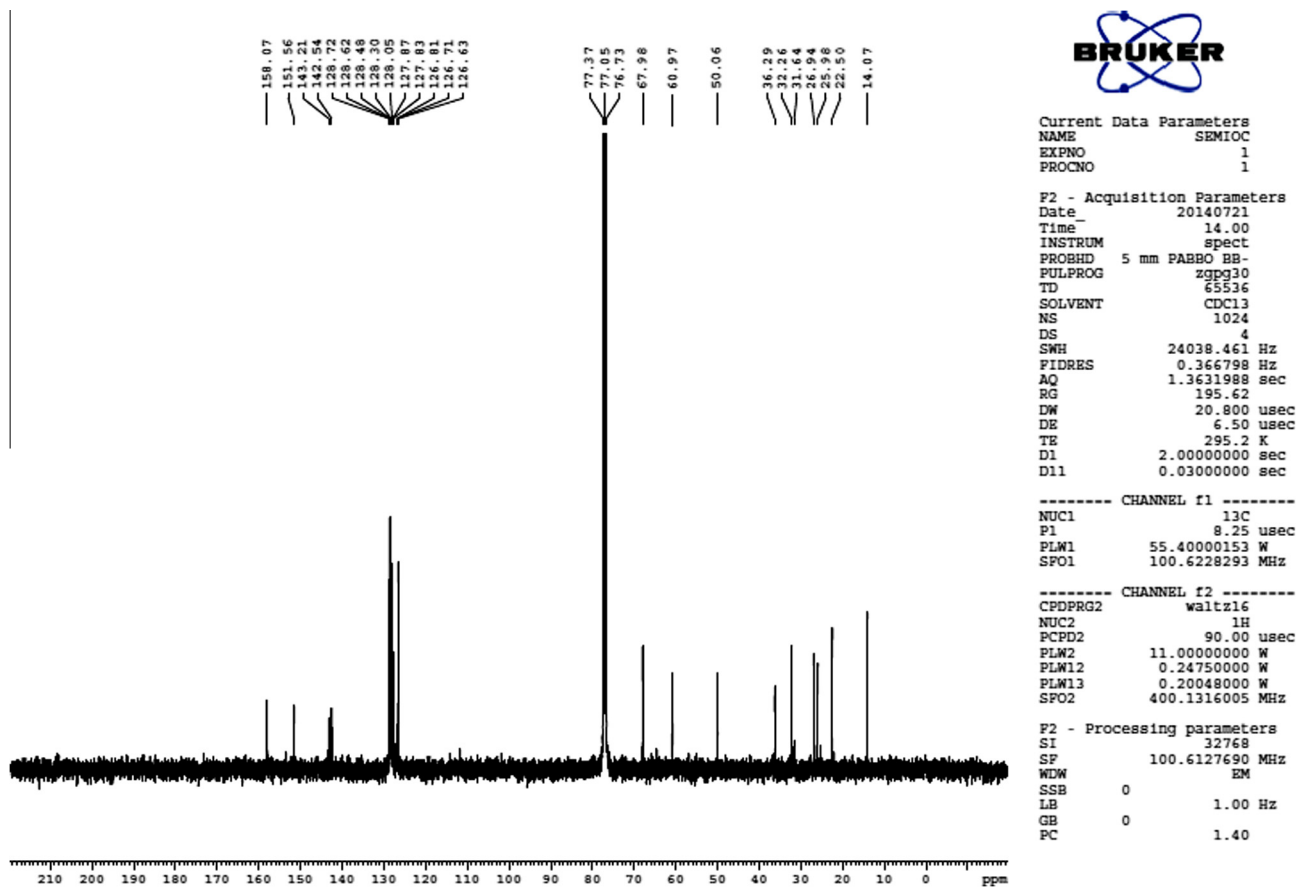
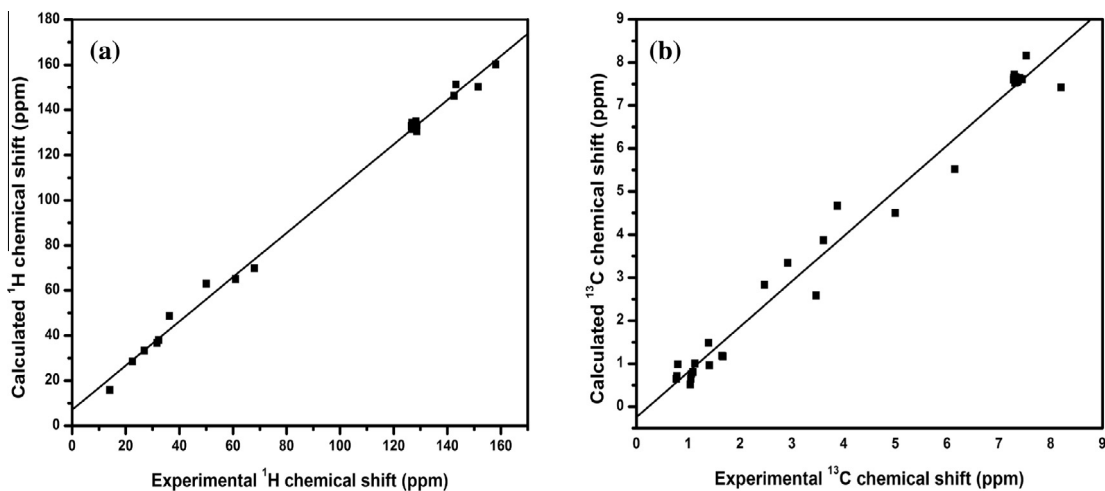
Atom	B3LYP 6-311G+(2d,p)	Experiment	Atom	B3LYP 6-311G+(2d,p)	Experiment
C1	69.70	67.98	H7	3.87	3.61
C2	62.99	50.06	H6	2.58	2.48
C3	150.2	151.56	H8	2.83	2.11
C4	48.71	36.29	H9	3.34	2.90
C5	64.98	60.97	H10	4.67	3.88
C13	146.33	142.54	H11	1.48	1.39
C14	133.27	128.48	H17	8.16	7.53
C15	132.45	127.83	H19	7.61	7.45
C16	133.38	128.7	H21	7.64	7.4
C18	132.51	128.05	H22	7.57	7.37
C20	131.52	126.71	H23	7.54	7.35
C24	151.29	143.21	H28	7.66	7.33
C25	130.57	128.62	H30	7.53	7.31
C26	134.9	128.3	H32	7.72	7.3
C27	134.04	127.89	H33	7.65	7.29
C29	134.29	126.81	H34	7.6	7.28
C31	132.76	126.63	H57	7.42	8.22
C53	160.18	158.07	H55	4.50	5.00
C35	33.29	26.94	H56	5.52	6.15
C38	36.71	31.64	H36	1.17	1.61
C41	37.95	32.26	H37	1.18	1.65
C44	22.50	22.50	H39	0.51	1.04
C47	15.79	14.07	H40	0.65	1.05
			H42	0.76	1.06
			H43	0.96	1.41
			H45	0.80	1.09
			H46	1	1.13
			H49	0.64	0.77
			H48	0.98	0.80
			H50	0.71	0.78

polarizability (α_{tot}) and the mean first hyperpolarizability (β_{tot}) values are 24.995×10^{-24} , 25.193×10^{-24} and 6.5662×10^{-31} , 6.6884×10^{-31} in B3LYP and HF levels theories, respectively and the values are presented in Table 5. Total hyperpolarizability of the molecule is approximately two times greater than those of urea [51] and 17 times greater than 3-hydroxy-2-naphthoic acid hydrazide [52]. Narayan et al. [53] reported hyperpolarizabilities of 5-nitro-2-furaldehyde semicarbazone less than that of urea. The above results show that PDPOSC can be best material for NLO applications.

NMR

The experimental and theoretical values for ^1H and ^{13}C NMR of PDPOSC are given in Table 6. The NMR spectra were recorded in CDCl_3 and presented in Figs. 6 and 7. The theoretical chemical shift values were calculated by GIAO method using B3LYP/6-311G+(2d,p) level theory. The two downfield signals (3.88 ppm doublet of doublet and 3.61 ppm doublet) are assigned to H10 and H7, respectively. The signal at 2.90 ppm, doublet of doublet is due to the H9 proton. Consequently, the signals at 2.48 and 2.11 ppm are due to H6 and H8, respectively. The most downfield singlet at 8.22 ppm is assigned to NH proton of semicarbazone group and the two downfield signals at 6.15 and 5.0 ppm are due to NH_2 protons of semicarbazone group. The aryl protons signal, around 7.26–7.54 ppm is a multiplet which is due to aromatic protons in phenyl ring carbons at C1 and C5. The multiplets around the region 0.80–1.61 ppm are assigned to the methylene protons of

**Fig. 6.** ^1H NMR spectrum of PDPOSC.

Fig. 7. ^{13}C NMR spectrum of PDPOSC.Fig. 8. The linear regression between the experimental and theoretical (a) ^1H and (b) ^{13}C chemical shifts of PDPOSC.

pentyl side chain at C2. The upfield triplet at 0.77 ppm is assigned to methyl proton of pentyl side chain.

Signals of aromatic carbons were observed in the range of 126.63–143.21 ppm. The upfield signals around 14.07 ppm is assigned to C47 and other upfield signals in the region 22.5–32.26 ppm are assigned to four methylene carbons of pentyl side chain at C2. The downfield signal at 151.56 ppm is assigned to C3

due to neighboring electronegative N51. The signal around 67.98 and 60.97 ppm are due to benzylic carbons at C1 and C5 and the remaining signals at 50.06 and 36.29 ppm are due to C2 and C4 carbons, respectively. The most downfield signal around 158.07 ppm is assigned to C=O carbon of semicarbazone group. The predicted chemical shift values are in good agreement with the experimental values.

Table 7

Calculated thermodynamic parameters of PDPOSC employing HF/ B3LYP/6-311++G(d,p).

parameter	B3LYP 6-311++G(d,p)	HF 6-311++G(d,p)
Total energy (a.u.)	-1189.04210	-1181.35579
Zero point energy (kcal mol ⁻¹)	312.51490	334.34195
Rotational constants (GHz)		
	0.21090	0.20326
	0.12092	0.12582
	0.08890	0.08940
Entropy (cal mol ⁻¹ k ⁻¹)		
Total	187.23	180.69
Translational	43.68	43.68
Rotational	36.20	36.19
Vibrational	107.34	100.81

The linear regression between the experimental and theoretical ¹H and ¹³C NMR Chemical shifts of PDPOSC are represented in Fig. 8a and b.

In the present study, the following linear relationships were obtained for ¹³C and ¹H chemical shifts.

For ¹³C

$$\delta_{\text{cal}} = 1.0533\delta_{\text{exp}} - 0.24887 \quad (R^2 = 0.99099)$$

For ¹H;

$$\delta_{\text{cal}} = 0.981\delta_{\text{exp}} + 7.0549 \quad (R^2 = 0.99805)$$

Correlation coefficients of ¹³C NMR and ¹H NMR were determined as 0.99099 and 0.99805, respectively for PDPOSC.

Thermodynamic analysis

The thermodynamic parameters such as zero-point vibrational energy, thermal energy, rotational constants and entropy of the compound have also been computed by B3LYP and HF methods with 6-311++G(d,p) basis set and are presented in Table 7. In the present investigation, the total energy as well as the zero-point vibrational energy of PDPOSC increases at room temperature and different methods also presented. Among the two methods, B3LYP/6-311++G(d,p) shows minimum total energy (-1189.0421 a.u) for the title compound.

The statistical thermodynamic functions like heat capacity (C_p), entropy (S) and enthalpy changes (ΔH) for PDPOSC were obtained

from the theoretical harmonic frequencies and listed in Table S4. From Table S4, it can be seen that these thermodynamic functions are increasing with temperature ranging from 100 to 1000 K due to the fact that the molecular vibrational intensities increase with temperature [54]. The correlation equations between heat capacity, entropy, enthalpy changes and temperatures were fitted by quadratic formulas and the corresponding fitting factors (R^2) for these thermodynamic properties are 0.9999, 0.9988 and 0.9990, respectively. The corresponding fitting equations are as follows and the correlation graphics are shown in Fig 9a and b.

$$C_p = 301.48 + 1.716T - 3.187 \times 10^{-4} T^2 \quad (R^2 = 0.9999)$$

$$S = 0.90103 + 1.730T - 6.66805 \times 10^{-4} T^2 \quad (R^2 = 0.9988)$$

$$H = -16.42 + 0.16555T + 5.04889 \times 10^{-4} T^2 \quad (R^2 = 0.999)$$

The above data can be used to compute other thermodynamic energies according to the well known relationships of thermodynamic functions and to predict directions of chemical reactions [55].

Conclusions

Overall, the piperidone ring is found to adopt chair conformation with equatorial orientation of substituents. Comparison of calculated and experimental vibrational spectral data show that the B3LYP/6-311++G(d,p) method gave comparable data, while HF/6-311++G(d,p) method gave data positively deviated and the optimized geometrical parameters show the lengthening of N54–H56 bond and shortening of C53–O58 bond due to the possibility of N54–H56...O58 hydrogen bonding. The NBO analysis obviously illustrates the stability of the molecular structure that arises from conjugative interactions, charge delocalisation and $E^{(2)}$ energies confirm the occurrence of intra-molecular charge transfer. Negative regions are associated with N51 and O58 atoms. Thus, it is predicted that the oxygen atom will be preferred electrophilic site. Positive regions are located on the carbon atom with a value around +0.487 a.u. indicating possible site for nucleophilic attack. The electronic transitions and states were investigated computationally by the application of TD-DFT theory and show good agreement with the experimental UV–vis absorption results. The calculated first hyperpolarizability of PDPOSC is two times greater than that of urea and so in future can be used as NLO material. A comparison of theoretical NMR spectra with the corresponding experimental ones shows a good agreement.

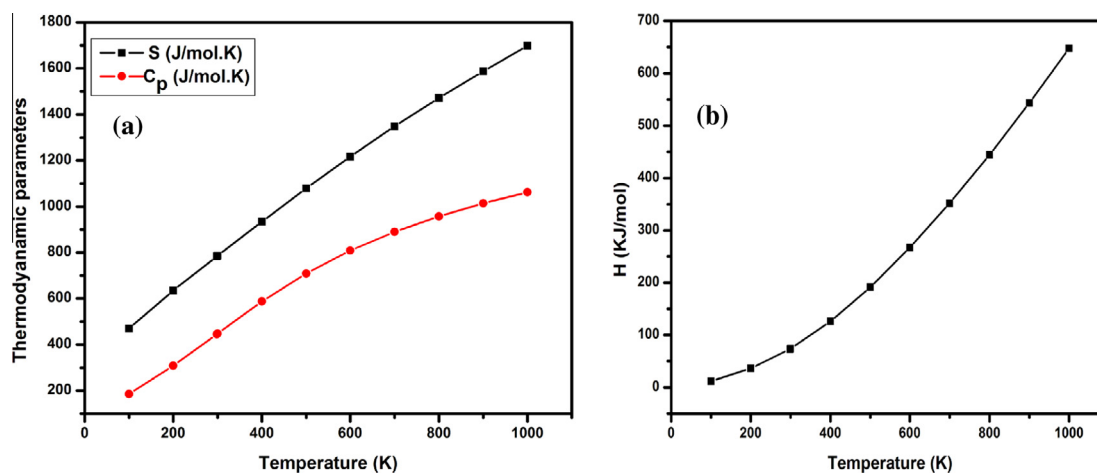


Fig. 9. (a) variation of entropy and heat capacity with temperature (b) variation of enthalpy with temperature.

Acknowledgments

One of the authors, Dr. G. Rajarajan is thankful to UGC [F. No. 42-343/2013 (SR)] for providing funds to this research study. Mr. M. Arockia doss is thankful to UGC for providing fellowship. The authors also wish to thank Dr. N. Jayachandramani, former Head, Department of Chemistry, Pachaiyappa's college, Chennai-30.

Appendix A. Supplementary data

Supplementary data associated with this article can be found, in the online version, at <http://dx.doi.org/10.1016/j.saa.2015.03.117>.

References

- [1] A.R. Kartrizky, *Comper. Heteocycl. Chem.* 5 (1995) 20–24.
- [2] H.I.E.L. Subbagh, S.M. Abu-Zaid, M.A. Mahran, F.A. Badria, A.M. Alafaid, *J. Med. Chem.* 43 (2000) 2915–2921.
- [3] A.A. Watsona, G.W.J. Fleet, N. Asano, R.J. Molyneux, R.J. Nugh, *Phytochemistry* 56 (2001) 265–295.
- [4] N. Rameshkumar, A. Veena, R. Ilavarasan, M. Adirja, P. Shanmugapandian, S.K. Sridhar, *Biol. Pharm. Bull.* 26 (2003) 188–193.
- [5] C.R. Ganellin, R.G.W. Spickett, *J. Med. Chem.* 8 (1965) 619–625.
- [6] M.X. Wei, L. Feng, X.Q. Li, X.Z. Zhou, Z.H. Sho, *Eur. J. Med. Chem.* 44 (2009) 3340–3344.
- [7] P. Parthipan, G. Aridoss, P. Rathika, V. Ramkumar, S. Kabilan, *Bioorg. Med. Chem. Lett.* 19 (2009) 6981–6985.
- [8] N. Vijayan, R. Ramesh babu, M. Gopalakrishna, R. Gopalakrishnan, P. Ramasamy, *J. Cryst. Growth* 233 (2001) 863–867.
- [9] R. Ramesh babu, N. Vijayan, R. Gopalakrishna, P. Ramasamy, *J. Cryst. Growth*, 244 (2002) 545–548.
- [10] K. Sethuraman, R. Ramesh babu, M. Gopalakrishna, R. Gopalakrishnan, P. Ramasamy, *J. Cryst. Growth* 290 (2006) 539–543.
- [11] D. Sajan, J. Binoy, B. Pradeep, K. Venkatakrishnan, V.B. Kartha, I. Hubert Joe, *Spectrochim. Acta Part A Mol. Biomol. Spectrosc.* 60 (2004) 173–180.
- [12] J.P. Abraham, I. Hubert Joe, V. George, O.F. Nielson, V.S. Jayakumar, *Spectrochim. Acta Part A Mol. Biomol. Spectrosc.* 59 (2003) 193–199.
- [13] S. Thennarasu, P.T. Perumal, *Molecules* 7 (2002) 487–493.
- [14] M.J. Frisch, et al., *Gaussian 03, Revision E.01*, Gaussian Inc, Wallingford, CT, 2004.
- [15] G. Rauhut, P. Pulay, *J. Phys. Chem.* 99 (1995) 3093–3100.
- [16] A.P. Scott, L. Radon, *J. Phys. Chem.* 100 (1996) 16502–16513.
- [17] D. Michalska, *Raint program*, Wroclaw university of Technology, 2003.
- [18] S. Subashchandrabose, H. Saleem, Y. Erdogdu, G. Rajarajan, V. Thanikachalam, *Spectrochim. Acta Part A Mol. Biomol. Spectrosc.* 82 (2011) 260–269.
- [19] A. Manimekalai, T. Maruthavanan, K. Selvaraju, *Spectrochim. Acta Part A Mol. Biomol. Spectrosc.* 97 (2012) 942–947.
- [20] G. Velraj, S. Soundharam, C. Sridevi, *J. Mol. Struct.* 1060 (2014) 156–165.
- [21] P. Gayathri, J. Jayabharathi, G. Rajarajan, A. Thiruvalluvar, R.J. Butcher, *Acta Crystallogr.* 65E (2009) o3083.
- [22] T.S. Chia, C.K. Quah, C.W. Ooi, B. Garudachari, N.A. Isloor, A.M. Isloor, H.K. Fun, *J. Chem. Crystallogr.* 44 (2014) 51–56.
- [23] A. Dhandapani, S. Manivarman, S. Subaschandrabose, H. Saleem, *J. Mol. Struct.* 1058 (2014) 41–50.
- [24] M. Barthes, G. De Nunzio, M. Ribet, *Synth. Met.* 76 (1996) 337–340.
- [25] R. Shanmugam, D.N. Sathyanarayana, *Spectrochim. Acta Part A Mol. Biomol. Spectrosc.* 40 (1984) 757–761.
- [26] M. Kurt, S. Okur, S. Demic, J. Karpagam, N. Sundaraganesan, *J. Raman Spectrosc.* 42 (2011) 1682–1689.
- [27] D. Sajan, I. Hubert Joe, V.S. Jayakumar, *J. Raman Spectrosc.* 37 (2005) 508–519.
- [28] M. Gussoni, C. Castiglioni, M.N. Ramos, M. Rui, G. Zerbi, *J. Mol. Struct.* 224 (1990) 445–470.
- [29] G. Socrates, *Infrared and Raman Characteristic Group Frequencies*, Wiley, New York, 2001.
- [30] V. Krishnakumar, V. Balachandran, *Spectrochim. Acta, Part A: Mol. Biomol. Spectrosc.* 63 (2006) 464–476.
- [31] V. Krishnakumar, R. John Xavier, *Indian J. Pure Appl. Phys.* 41 (2003) 95–98.
- [32] K. Furic, V. Mohacek, M. Bonifacic, I. Stefanic, *J. Mol. Struct.* 267 (1992) 39–44.
- [33] C. Yohannan Panicker, Asha Raj, Hema Tresa Varghese, K. Rajud, Y. Sheena Mary, *J. Raman Spectrosc.* 41 (2010) 829–838.
- [34] M. Szafran, A. Komasa, E.B. Adamska, *J. Mol. Struct.* 827 (2007) 101–107.
- [35] C. James, A. Amal Raj, R. Reghunathan, I. Hubert Joe, V.S. Jayakumar, *J. Raman Spectrosc.* 37 (2006) 1381–1392.
- [36] J.N. Liu, Z.R. Chen, S.F. Yuan, *J. Zhejiang Univ. Sci. B* 6 (2005) 584–591.
- [37] C. Ravikumar, I. Hubert Joe, V.S. Jayakumar, *Chem. Phys. Lett.* 460 (2008) 552–558.
- [38] N. Rameshkumar, R. Ilavarasan, *Biol. Pharm. Bull.* 26 (2003) 188–193.
- [39] E. Scrocco, J. Tomasi, *Adv. Quant. Chem.* 11 (1978) 115–121.
- [40] F.J. Luque, J.M. Lopez, M. Orozco, *Theor. Chem. Acc.* 103 (2000) 343–345.
- [41] N. Okulik, A.H. Jubert, *Internet Electron. J. Mol. Des.* 4 (2005) 17–30.
- [42] K. Fukui, T. Yonezawa, H. Shingu, *J. Chem. Phys.* 20 (1952) 722–725.
- [43] H. Ghalla, N. Issaoui, M. Govindarajan, H.T. Flakus, M.H. Jamroz, B. Oujia, *J. Mol. Struct.* 1059 (2014) 132–143.
- [44] N. Vijayan, R.R. Babu, R. Gopalakrishnan, S. Dhanuskodi, P. Ramasamy, *J. Cryst. Growth* 236 (2002) 407–412.
- [45] L. Jothi, K. Ramamurthi, *Ind. J. Sci. Technol.* 4 (2011) 666–669.
- [46] S.I. Gorelsky, *SWizard Program Revision 4.5*, University of Ottawa, Ottawa, Canada, 2010.
- [47] Y.X. Sun, Q.L. Hao, W.X. Wei, Z.X. Yu, L.D. Lu, X. Wang, Y.S. Wang, *J. Mol. Struct.:(Theochem.)* 904 (2009) 74–82.
- [48] C. Andraud, T. Brotin, C. Garcia, F. Pelle, P. Goldner, B. Bigot, A. Collet, *J. Am. Chem. Soc.* 116 (1994) 2094–2102.
- [49] M. Nakano, H. Fujita, M. Takahata, K. Yamaguchi, *J. Am. Chem. Soc.* 124 (2002) 9648–9655.
- [50] V.M. Geskin, C. Lambert, J.L. Bredas, *J. Am. Chem. Soc.* 125 (2003) 15651–15658.
- [51] Z.M. Jin, B. Zhao, W. Zhou, Z.H. Jin, J. Powder Diff. 12 (1997) 47–48.
- [52] J. Karpagam, N. Sundaraganesan, S. Sebastian, S. Manoharan, M. Kurt, *J. Raman Spectrosc.* 41 (2010) 53–62.
- [53] V. Narayan, H.N. Mishra, O. Prasad, L. Sinha, *Comput. Theor. Chem.* 973 (2011) 20–27.
- [54] J. Bevan Ott, J. Boerio-Goates, *Calculations from Statistical Thermodynamics*, Academic Press, 2000.
- [55] R. Zhang, B. Dub, G. Sun, Y. Sun, *Spectrochim. Acta Part A Mol. Biomol. Spectrosc.* 75 (2010) 1115–1124.